AD-A191 818 THE HYDROTHERMAL DISSOLUTION OF PEROVSKITE (CATIO3)(U) 1/1
ATOMIC ENERGY RESEARCH ESTABLISHMENT HARWELL (ENGLAND)
S MYHRA ET AL. NOV 86 AERE-R-12390

UNCLASSIFIED F/G 8/7 NL

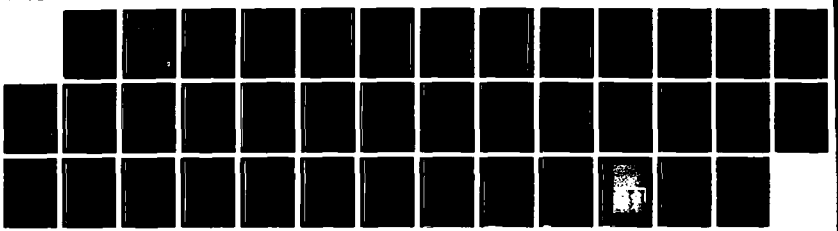

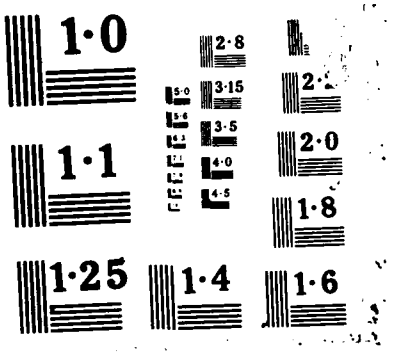
1·0
1·1
1·25
1·4
1·6
1·8
2·0
2·8
3·15
3·5
4·0
4·5

AERE R 12390

APPROVED FOR PUBLICATION

AERE R 12390

THIS DOCUMENT IS INTENDED FOR PUBLICATION IN THE OPEN LITERATURE
Until it is published, it may not be circulated, or referred to outside the organisation to which copies have been sent.

United Kingdom Atomic Energy Authority

HARWELL

The hydrothermal dissolution of perovskite ($CaTiO_3$)

S Myhra, H E Bishop and J C Rivière

Materials Development Division
Harwell Laboratory, Oxfordshire OX11 0RA

November 1986

C22

APPROVED FOR PUBLICATION

THE HYDROTHERMAL DISSOLUTION OF PEROVSKITE ($CaTiO_3$)

S. Myhra*, H E Bishop, J C Riviere
and N Stephenson**

ABSTRACT

Perovskite ($CaTiO_3$) has been exposed to hydrothermal chemical attack in aqueous solution. Dependence on temperature (150-250°C) and on duration of attack (1 to 35 days) have been investigated. It was found that a precipitate surface layer was formed. The thickness of this layer ranged from a few monolayers to several hundred nanometers for the least and the most severe hydrothermal conditions, respectively. The composition of the layer, as deduced by surface analytical techniques, suggests that (i) there is congruent dissolution of the perovskite surface, (ii) a TiO_2 precipitate layer is formed, and (iii) the presence of silica and CO_2 in solution do not appear to affect substantially the mechanism of the rate of dissolution.

Key Words: Perovskite, Nuclear Waste Disposal, Hydrothermal Dissolution, Surface Analysis

*Permanent address: School of Science, Griffith University, Nathan, Queensland, Australia

**School of Science, Griffith University, Queensland

Materials Development Division
Harwell Laboratory

November 1986

HL86/1436 (C22)

CONTENTS

TABLES

ILLUSTRATIONS

Illustrations - Continued

Figure 3a, b Abundances of (a) Ca and Si, and (b) Ti and O as functions of ion etching dose. The effect of temperature is investigated. 200 hrs at 150°C in DDW + SiO_2 (R6) = •, 250 hrs at 175°C in DDW + SiO_2 (R3) = 0; 168 hrs at 250°C in DDW + SiO_2 (R9) = x; 670 hrs at 250°C in DDW + SiO_2 (R8) = □.

Figure 4 Binding energies of O 1s, Ti $2p_{3/2}$, C 1s and Si 2p electrons as functions of ion etching dose for an unleached specimen (R0) = •; (R1) = 0; (R2) = ■; (R3) = □; and (R4) = x. Run conditions are listed in Table 1 and in caption for Figure 1.

Figure 5a, b Binding energies as functions of ion etching dose. R6 = • and (R7) = 0; are shown in (a) and (R3) = 0; (R6) = •; (R8) = □ and (R9) = x are shown in (b). Run conditions are listed in Table 1 and Figures 2 and 3.

Figure 6 Evolution of O 1s envelope as function of ion etching dose for R8, showing charge shifted peak due to either the presence of precipitated titanate on attacked surface, or a precipitated siliceous layer.

Figure 7 Experimental Ti 2p envelopes for a (a) polished unleached surface (R0), (b) 300°C for 455 hrs in DDW (R1) and (c) 175°C for 250 hrs in DDW + SiO_2 (R3) after ED = 100 μAmin.

Figure 8a, b SEM micrographs of fracture face of perovskite (R10) after 7 days in DDW at 250°C. (a) and (b) show the fracture face before and after polishing.

Figure 9 AES point scans on perovskite fracture face. Top scan is for P1 (Figure 8a) in the perovskite substrate, middle scan is for P2 at the substrate/precipitate interface and the bottom scan is for P3 in the precipitate layer.

INTRODUCTION

Perovskite is one of the major phases in the mineral assemblage known as Synroc C which has been proposed by Ringwood [1] as a matrix for disposal of high-level nuclear waste (HLW) from the light water reactor fuel cycle. The Synroc C waste form has exhibited excellent chemical durability under a variety of extreme hydrothermal conditions [2]. These studies have not sought to simulate actual repository conditions although the effects of many other variables such as temperature, pressure, pH and time have been investigated. It has been pointed out by Nesbitt et al. [3] however, that Ca-perovskite (and its Sr and Ba analogues) are thermodynamically unstable (although there may be kinetic constraints) in many natural groundwaters - especially if these contain either dissolved CO_2 or aqueous silica in solution. There are several possible reactions:

$$CaTiO_3 + CO_2(g) = TiO_2 + CaCO_3 \quad (1)$$

$$CaTiO_3 + SiO_2\,(aq) = CaTiSiO_2 \quad (2a)$$

$$\text{or } TiO_2 + Ca^{2+} \text{ silica gel} \quad (2b)$$

$$CaTiO_3 + H_2O = TiO_2 + Ca(OH)_2 \quad (3a)$$

$$\text{or } TiO_2 + Ca^{2+} + 2OH^- \quad (3b)$$

The hydrothermal decomposition reaction of $CaTiO_3$ in the presence of CO_2 in the fluid, to TiO_2 and $CaCO_3$, has been the subject of a

previous study of surface alterations of several titanate minerals [4]. The present study focusses on the two latter mechanisms whereby perovskite and silica in a hydrothermal environment may react to form either sphene ($CaTiSiO_5$) or TiO_2. Surface analytical techniques have been used to identify the rates and products of the fluid/solid interface reactions. X-ray Photoelectron Spectroscopy (XPS) and Auger Electron Spectroscopy (AES) have proven especially powerful because they have depth resolutions of 5–20 Å and are able to provide "chemical" information. AES has the additional virtue of providing lateral resolution in the sub-μm range. Thus it can help to identify precipitate phases. These techniques have been validated by earlier work on titanates and on Synroc [5, 6]. The information thus obtained can be related more directly to the effects of aqueous attack on the solid matrix than can that obtained from solution analysis and from other analytical techniques such as Electron Probe X-ray Microanalysis (EPMA) or SEM/EDS which have depth resolutions of the order of 1 μm.

EXPERIMENTAL AND ANALYTICAL TECHNIQUES

The specimen material was obtained from Anzon Ltd., Newcastle-upon-Tyne, UK, as monolithic discs. The manufacturer reported that these had been prepared by cold pressing and sintering Analar grade reagents at 1300°C for 2 hours. X-ray diffraction showed that there were no detectable minor phases at < 1% level of detectability. However, optical and SEM microscopy revealed substantial open porosity. One surface of each specimen was polished to a 1 μm diamond paste finish and cleaned ultrasonically in methanol to ensure that initial surface conditions were always identical.

The monolithic specimens (≈ 1 cm diameter and ≈ 2 mm thickness) were loaded into a Parr hydrothermal reaction vessel ("bomb") (lined with Teflon) with 20 ml of Analar distilled deionized H_2O (DDW); the geometrical specimen surface area to leachant volume ratio, A/V, was therefore about 10^{-3} m^{-1}. Finely divided CAB-O-SIL SiO_2 powder (≈ 1 μm mean diameter) was included in an amount sufficient to ensure that the solution would always be saturated with respect to amorphous silica. It is likely that the vessel and its contents reached the preset temperature of the oven within two hours, although the interior temperature of the reaction vessel could not be monitored, while the vessel could be quenched to laboratory ambient in less than 15 mins at the end of a run. After extraction from the vessels the specimens were cleaned ultrasonically in acetone in order to remove, as far as possible, absorbed water and SiO_2 adhering to exterior surfaces and interior pores. Experiments using the Parr vessels were carried out at 150°C and 175°C. The temperature range was extended to 250°C by using a large stainless steel vessel (no Teflon liner) with a volume of 1 litre. This vessel had a longer time-constant for heating and quenching, but the uncertainty in the duration of the effective time at temperature was at most no more than 10%. The DDW was similarly saturated with finely divided SiO_2 powder. One experiment was also carried out by enclosing the perovskite specimen and DDW in a silver bag, which was then loaded into the stainless steel vessel. In this case A/V was about $5 \times 10^{-4} m^{-1}$.

Distilled water in an open container will readily and rapidly absorb CO_2 from the atmosphere. Thus, a normal dissolution run will de

facto expose a specimen to CO_2 in solution. It is possible that the presence of CO_2 may affect reaction paths (2) and (3). Therefore one run, using a Parr vessel, was carried out in such a way as to exclude CO_2. This was done by allowing the open, but loaded, vessel to boil vigorously, in order to drive off the CO_2 and then sealing the hot vessel.

Pre- and post-attack features of the polished surfaces were studied by XPS and AES. Three different spectrometers were used, viz. at Harwell VG ESCALAB Mk. I and Mk. II instruments with hemispherical energy analysers, and at the Brisbane Surface Analysis Facility (BSAF) a PHI Model 560 instrument with a double pass cylindrical mirror analyser. The XPS capabilities of the spectrometers were roughly comparable while high spatial resolution AES could be carried out only on the ESCALAB Mk. II instrument. Selected spectral peaks for all atomic species Ca, Ti, Si, C and O were monitored. Ion beam etching was carried out to depths of up to 150 nm and scans were obtained at selected depth intervals. The areas under the selected peaks were determined and accepted sensitivity factors [7] were used to determine elemental abundances. Also, the peak positions by XPS were determined to an accuracy of ± 0.2 eV while peak envelopes were monitored in order to gain further information about the chemical state and environment of each species. Typical XPS instrumental parameters were as follows for the two spectrometers, those for the PHI instrument being shown in parenthesis. Survey scans at low resolution were characterised by a constant analyser pass energy of 100 eV, scan increments of 1 (0.5) eV and a scanning rate of 1 (20) increment s^{-1}. Detailed scans over individual peaks (O 1s, Ca 2p, Ti 2p, C 1s, Si 2s and Si 2p) used a pass energy of 50 (25) eV, increments of 0.2 eV and scan rates of 0.2-0.5 (20) increments s^{-1}. The

VG data were obtained from a single scan while in the case of the PHI instrument many scans were averaged. The working vacuum was 10^{-9} torr or better, extreme UHV conditions not being required for the non-reactive surfaces. Considerable charging was experienced for the fresh surfaces (shifts of up to 5 eV in the O 1s peak position were not uncommon). Ion beam etching and its attendant radiation damage tended to increase the surface conductivity and to eliminate charging; a dose of 30 μA min-cm^{-2} of 5 keV Ar^+ ions was usually sufficient. The C 1s peak is not a reliable energy marker for these materials since carbon occurs both as an unavoidable graphitic contaminant and as carbonates in the surface in accord with reaction path (1). Graphitic contamination is universally present at the monolayer level unless clean surfaces have been prepared under extreme UHV conditions. In addition, the state of ceramic technology is such that graphitic contamination will be present in the bulk for those particular specimens. However, previous work has shown that the Ca $2p_{3/2}$ peak does not shift much, after surface contamination has been removed, from a position corresponding to a binding energy of 347.8 eV irrespective of ion dose, the type of titanate and the condition of the surface. This peak was therefore used as an energy marker in the present work. The instrumental parameters for acquisition of AES data were: constant retard ratio of 4; increments of 0.5 and 1.0 eV, respectively, below and above 1000 eV kinetic energy; 10 keV primary electron energy; beam current of 3 nA; beam diameter $\lesssim$ 0.5 μm.

RESULTS

The essential parameters for the relevant runs are listed in Table 1. Survey scans were obtained of surfaces before attack, after attack in DDW and after attack in DDW saturated with silica and CO_2. The major peaks were identified. It was immediately evident that the effect of the hydrothermal environment was to produce a surface with a lower calcium concentration and to introduce silicon. Figures 1a and b show the concentration profiles for all major species as functions of ion dose, ΣD, for an as-received specimen and specimens attacked in DDW (R1) and in DDW + SiO_2 + CO_2 for 30 (R2), 250 (R3) and 525 (R4) hours. Based on previous experience it is likely that 1 μAmin ion dose is roughly equivalent to a removal of 0.2 nm of surface material [5,6]. The nominal stoichiometries of $CaTiO_3$ and $CaTiSiO_5$ are shown for comparison. The effect of dissolved CO_2 on the chemical attack at 150°C is shown in Figure 2a and b. The two runs (R6 and R7) were roughly comparable insofar as the temperatures were identical although the durations differed by a factor of three. The major differences appear to be in the Ti profiles. This species was substantially depleted in the absence of dissolved CO_2 while some enrichment in the near surface layers occurred when CO_2 was present. Somewhat surprisingly it was found that the carbon abundances were roughly comparable for the two runs. These are not plotted in Figure 2 but ranged from about 25 at.% coverage for integrated ion doses of $\sum D$ = C to about 10% for ΣD = 500 (see Table 2). It is therefore likely that the major source of carbon was due not to dissolved CO_2 but rather to adventitious surface and bulk contamination of the specimen. For instance, we have found that exposed titanate surfaces take up CO_2 from the atmosphere. The temperature dependences

of the profiles are shown in Figures 3a and b which show data from R6 (150°C), R3 (1975°C) and R9 (250°C). The major differences were again found for the Ti profiles where the enriched layers were found at ED ~ 25, 60, 200 for 150, 175 and 250°C, respectively. Also, Ti became increasingly depleted with higher temperature in the first few monolayers. There was a slight trend towards increasing depth of depletion for Ca with increasing temperature, although R9 (250°C and 168 hrs) went against that trend. Similarly, the trend for Si was that of a slight increase in concentration with temperature. Finally, carbon tended to be concentrated more in the first few monolayers at 250°C in comparison with runs at lower temperature, Table 2. Results for R8 (longer duration than R9) have been included in Figure 3; it can be seen that the Si concentration increased very substantially with time while Ti and Ca were correspondingly depleted.

In Figure 4 are shown the XPS binding energies corresponding to the peak positions of Ti $2p_{3/2}$, O 1s, C 1s and Si 2p versus ion dose for the same runs as the data in Figure 1. The effects of dissolved CO_2 and temperature on the binding energies of these species are shown in Figure 5a and b. The binding energies have been corrected for charging by setting the Ca $2p_{3/2}$ binding energy equal to 347.8 eV, the binding energy of this level is relatively invariant for all compounds which are likely to be present. Typical binding energies for the relevant atomic species are listed in Table 3.

Peak envelopes were obtained as functions of surface treatment and ion dose. The Si 2p envelopes did not exhibit any unusual features. The Ca 2p envelopes tended to be better resolved for more severe attack

when compared to those obtained for lower temperature and shorter duration. The O 1s envelopes exhibited some high binding energy contributions; in Figure 6 are shown O 1s envelopes for R8. Other runs of lesser hydrothermal severity exhibited smaller high-binding energy contributions. The Ti 2p envelope before ion etching was substantially similar for all surface conditions (polished, DDW and DDW + SiO_2 attack). The envelope showed the well-known trend with increasing ion dose whereby the initially predominant tetravalent character of the envelope would acquire contributions from states of lower valency. It was found that the surface exposed to silicated DDW was considerably more affected by bombardment than any other surface. This is shown in Figure 7 for the Ti 2p envelope after an ion dose of 100 μAmin.

The specimen from R10 was investigated by SEM and AES. After 7 days in DDW at 250°C a precipitate layer was clearly visible to the naked eye. The specimen was fractured in order to study the details of this layer and its relationship to the underlying perovskite matrix. Figure 8a shows an SEM image of the fracture face. The precipitate layer is clearly visible and there is a distinct interface. This face was polished in order to highlight the contrast between the precipitate layer and the perovskite substrate, Figure 8b. High spatial resolution AES point scans were carried out along a line perpendicular to the interface. Data obtained at points labelled 1, 2 and 3 in Figure 8a are shown in Figure 9.

DISCUSSION

Elemental Abundances

In general, the trend is for Ca to be increasingly depleted in the post-attack surface layers with increased duration of attack and with temperature. Ti is also depleted, but only in the near-surface layers; deeper into the post-attack surface there is a pronounced enrichment. These features persist to progressively greater depths with increasing duration and temperature of attack. The trend for Si is to exhibit greater concentration and deeper penetration with time and temperature. Similarly, the O concentration is enhanced in the post-attack layer and the enhancement is more prounounced with time and temperature. Finally, carbon is enhanced in the near-surface layer but is depleted in the bulk by increasing duration and temperature, Table 2. The trend for C is not entirely systematic, presumably because the supply and chemical state of this species in solution are not well-controlled variables.

Binding Energies and Peak Shapes

The binding energies of the Ti 2p electrons are affected by radiation damage associated with ion bombardment; the reduction in titanates of tetravalent Ti to species of lower valencies with increasing ion dose has been discussed elsewhere [5, 6]. For instance, it has been found that zirconolite and hollandite are less resistant to bombardment than perovskites (in terms of propensity for Ti to be reduced). The present data show that the post-attack surface layer contains Ti in a structure which is relatively more vulnerable to bombardment than perovskite. This is also evident from consideration of the Ti 2p envelopes in Figure 7.

Surface Si has a binding energy (2p peak) of 103.5 to 104.0 eV, which is characteristc of SiO_2; a binding energy of 104 eV may be indicative of the presence of Si gel. However, it exhibits a lower binding energy, about 102.8 eV, in the remainder of the post-attack layer. The latter binding energy is that commonly observed for the Si 2p electrons in silicates; SiO_x, with $0 \leq x < 2$, is thought to have a 2p binding energy which decreases from 103.5 eV with decreasing x until 99 eV is reached for elemental silicon [8]. It is likely that Si occurs as a hydrated gel species in the post-attack surface layer; this interpretation is in accord with a 2p binding energy below that of crystalline SiO_2. Likewise, the high binding energy component of the O 1s peak at 534 eV is consistent with the inferred presence of a silicaceous layer. However, the high energy component O 1s may also be due to charge shifting of precipitated TiO_2 regions. The Ca 2p envelope and binding energy are not significantly affected by bombardment or severity of chemical attack. Similarly, the Si 2p envelope does not exhibit any unusual features.

The binding energy corresponding to the C 1s peak in general is about 286 eV for ED = 0. The trend is then that this energy drops to around 285 eV inside the post-attack layer. The exception is for R3, R4 and, in part, R8 for which high binding energy carbon persists throughout the post-attack layer. However, these observations may not be relevant or significant since the presence of carbon in the system cannot readily be controlled.

The O 1s peak position and shape after attack at 250°C exhibit contributions from either a high binding energy species or from a charge shifted surface feature. Thus it could be due to either oxygen being

present in a silica gel layer and/or precipitated TiO_2 crystallites on the surface. These contributions are enhanced with the duration and severity of the chemical attack. At 150 and 175°C there are no variations within the error bars except for the normal slight increasing in binding energy for $\Sigma D = 0$ as a result of surface hydroxylation.

Structure of Precipitate Layer

XPS, AES and SEM analyses provide no direct information about the structure of surface layers. However, these techniques do offer indirect evidence for the presence or absence of particular structures. For XPS and AES the experimental abundances may be related to expected stoichiometries, and the observed XPS binding energies may be consistent with the chemical environment of a particular species in a certain crystal structure. The morphology of precipitate crystallites, as determined by SEM, may also suggest the presence of a particular structure. In principle, one might expect $CaCO_3$, TiO_2, $CaTiSiO_5$ and SiO_2 to be present as crystalline precipitates on the $CaTiO_3$ substrate. Amorphous silicaceous and titanaceous layers may also be present.

The combined evidence from XPS, AES and SEM suggests that the post-attack perovskite surface is partially or fully covered with TiO_2 and a thin silicaceous layer. Calcium carbonate and $Ca(OH)_2$ may also be present. The atomic concentration profiles, the charge shifted C 1s peak and the SEM features indicate that TiO_2 is the dominant precipitate. Even though XPS, and AES to some extent, will average out the localized effects of TiO_2 crystallites over the whole surface area,

it is clear that the effects of precipitation increase with increasing severity of attack. In the first few monolayers O, Si and C are enriched while Ti and Ca are substantially depleted. These layers are therefore likely to consist of silica gel, hydrated species and carbon contaminants.

The crystallography of the TiO_2 precipitates has been investigated in a series of separate, but related, experiments. Ion beam thinned perovskite foil specimens suitable for transmission electron microscopy (TEM) have been studied at Griffith University [9] and at the Australian Atomic Energy Commission [10]. Such foils have been subjected to hydrothermal attack (150-190°C, 1-6 days) in aqueous solutions (DDW and DDW + SiO_2) in Parr reaction vessels. It has been found that TiO_2 grows as a precipitated crystalline phase on such specimens; using selected area diffraction (SAD) and EDS, these crystallites have been indexed and analyzed as brookite (DDW) and mixed brookite/anatase (DDW + SiO_2). It has been found that the extent of growth increases with temperature and duration. Conversely, sphene, calcite or silica-bearing phases are not found by TEM/SAD/EDS.

Mechanisms

The following equilibria are relevant to the nature of perovskite dissolution in DDW saturated with dissolved silica and containing CO_2:

$$CaTiO_3 + CO_2 = TiO_2 + CaCO_3 \quad (4)$$

$$CaTiO_3 + H_2O = TiO_2 + Ca(OH)_2 \quad (5)$$

$$CaTiO_3 + SiO_2 = CaTiSiO_5 \quad (6)$$

Earlier work on $CaTiO_3$ in CO_2-bearing DDW [4] has shown that the dissolution may proceed as follows:

(i) Selective leaching of Ca^{2+} coupled with hydration of the surface layers.

(ii) Saturation of calcium carbonates in the fluid phase and ultimately precipitation on the specimen surface (and elsewhere).

(iii) Attainment of final equilibrium so that the partial pressure of CO_2 is reduced to an extent that $CaTiO_3$, carbonates, CO_2 in solution and Ca^{2+} in solution become part of a self-buffered system.

The stability of sphene in various aqueous media is clearly relevant to considerations of the chemical durability of perovskite. Sphene has been investigated by Hayward et al. [11]. They have shown that for the system H^+-H_2O-CaO-TiO_2-SiO_2 it can be argued on thermodynamic grounds that (a) $CaTiO_3$ is the most stable phase for a silica concentration much below saturation and when $K = \log([Ca^{2+}]/[H^+]^2)$ is high, (b) TiO_2 is favoured when K is very low and (c) $CaTiSiO_5$ is favoured for saturation of silica and high K. Similarly, Nesbitt et al. [3] have shown that, with carbonate in solution, perovskite is stable only in groundwater with high K and low silica concentrations.

Finally, Hayward et al. [11] have also considered the stability of $CaSiTiO_5$ in the presence of carbonates in solution. They show that $CaSiTiO_5$ is the stable phase at all temperatures above 25°C. The trends of the experimental results are that $CaSiTiO_5$ specimens exposed to synthetic groundwater and $CaO-TiO_2-SiO_2$ frit in solution at 100°C generally gain weight and that precipitates form on the surface. These precipitates are found to have the same morphology as sphenes.

Detailed leaching studies by solution analysis have been carried out by Ringwood [12] on the Synroc mineral assemblage which contains perovskite as one of its major constituent phases. In these studies it was found that the leach rates of Ca at the extreme temperature of 950°C in DDW were typically of order 10^{-2}-10^{-3} gm/m^2-day while the rates for Ti were near or below the limits of detectabilty ($\approx 10^{-4}$ gm/m^2-day). Similar measurements after hydrothermal attack at 200°C showed that the leach rates of Ca increased to 10^{-1}-10^{-2} gm/m^2-day while the rates for Ti were unchanged. These observations have led Ringwood to propose a mechanism whereby divalent elements, such as Ca, are selectively leached out of near-surface layers, leaving "skins" enriched in TiO_2.

There is a further piece of evidence which may have a bearing on the question of mechanisms. The total hydrothermal system with respect to mobilization and destination of species can be fully characterized by analysis of the solid surface, by analysis for species in solution, by investigations of the surfaces of the hydrothermal enclosure and, in the case of silica being present, by studies of solids suspended in solution We have carried out a limited number of such investigations of the total system. It has been found, for instance, that CAB-O-SIL in solution

does not provide a substrate for precipitation of species in solution. However, on the walls of the hydrothermal enclosure are found, by SEM/EDS and XPS, a significant amount of Ca (usually as a precipitated calcium phosphate; the phosphorus is present as a trace impurity). Similarly, the extent to which TiO_2 is present on the surfaces of the specimen can be used to determine the extent of dissolution of the perovskite matrix. The extent of dissolution may then be compared to the total amount of extracted Ca in the system in order to determine the relative importance of leaching versus dissolution. Within large experimental uncertainties it was found that the total rate of extraction of Ca from the specimen was consistent with the dissolution being congruent.

The following model may now be proposed.

(i) The net effect of hydrothermal attack is that dissolution is essentially congruent although preferential extraction of Ca by ion exchange may occur during the early stages of the dissolution process. For instance, it may be that Ca is extracted from the perovskite on a monolayer by monolayer basis, followed by collapse of the perovskite structure and subsequent recrystallization of TiO_2. Alternatively, the perovskite matrix may be dissolved by base catalyzed hydrolysis, leading to release of Ca and precipitation of TiO_2.

(ii) Titanium and its compounds are extremely insoluble in aqueous solutions. Thus one would expect that dissolution of the

perovskite matrix will be followed by precipitation of titanates. The present evidence shows that TiO_2 (as brookite in DDW leachant and brookite and anatase in DDW + SiO_2 leachant) is favoured over sphene, even when the leachant is saturated by silica. It is possible that Ti in solution is confined to the local region of the double layer at the solution/solid interphase while Ca is free to equilibrate throughout the solution volume. Thus the local region of the double layer may be super-saturated with respect to TiO_2 while undersaturated with respect to sphene. For long duration and high temperature, R8, it is found that the Si concentration exceeds 10 at.% with a depth of penetration greater than 10 nm. This particular hydrothermal regime may therefore be a candidate for the formation of sphene in accord with Nesbitt et al. [3].

(iii) The rôle of carbonates has been established in an earlier study and present indications are that there are no synergistic effects with the rôle of silica in solution. Likewise, the apparent effects of silica in solution are relatively minor insofar as the rate of dissolution and precipitation is not strongly dependent on this variable. However, it is possible that precipitation of sphene may be favoured at higher temperatures and longer durations.

ACKNOWLEDGEMENTS

This work was supported in part by the AERE Harwell Underlying Research Programme and by a grant from the Australian National Energy Research, Development and Demonstration Programme. One of the authors (S. Myhra) is grateful for the support and hospitality extended by the Surface Analysis Section, AERE. Experimental assistance from Mr. R. Bartram and Dr. L. Welch at AERE and from Mr. B. Wood of the BSAF is especially acknowledged. Several suggestions from Dr. D. Savage (British Geological Survey) were most helpful. We are indebted to Ms. T. Kastrissios, Dr. P.S. Turner and Dr. T.J. White for permission to quote unpublished results.

REFERENCES

1. A.E. Ringwood, "Safe Disposal of High Level Nuclear Reactor Wastes: A New Strategy". (Australian National University Press, Canberra, 1978).

2. K.D. Reeve, D.M. Lavins, E.J. Ramm, J.L. Woolfrey, and W.J. Buykx in: Topp, S. (ed.), Scientific Basis for Nuclear Waste Management IV (Elsevier, New York, 1982).

3. H.W. Nesbitt, G.M. Bancroft, W.F. Fyfe, S.N. Karkhanis, A. Nishijima, A. and S. Shin, Nature 289 (1981) 358.

4. S. Myhra, D. Savage, A. Atkinson, A. and J.C. Rivière, American Mineralogist 69 (1984) 902.

5. S. Myhra, H.E. Bishop, and J.C. Rivière, Surf. Technol. 19 (1983) 145.

6. S. Myhra, H.E. Bishop, and J.C. Rivière, Surf. Technol. 19 (1983) 161.

7. D. Briggs and M.P. Seah, (eds.) "Practical Surface Analysis by Auger and X-Ray Photoelectron Spectroscopy" (Wiley, 1983).

8. D.A. Stephenson and N.J. Binkowski, J. Non-Cryst. Sol. 22 (1976) 399.

9. T. Kastrissios, M. Stephenson, P.S. Turner and T.J. White, Proc. XI Intl. Congress on Electron Microscopy, Vol. 2, (Eds. T. Imura, S. Maruse and T. Suzuki), JSEM, Tokyo, 1986.

10. T. Kastrissios, M. Stephenson, P.S. Turner and T.J. White, "Dissolution of Perovskite - Implications for Synroc Formulations", (Submitted to J. Am. Ceram. Soc., 1986).

11. P.J. Hayward, I.E. Doern, E.V. Cecchetto and S.L. Mitchell, Canadian Mineralogist 21 (1983) 611.

12. A.E. Ringwood, Rept. No. 3907, "Nuclear Waste Immobilization in Synroc", NERDDP/EG/84/307 (Australian Govt. Printing Off. 1984).

13. C.N. Sayers and N.R. Armstrong, Surf. Science 77 (1978) 301.

14. H. Van Doveren and J.A.Th. Verhoeven, J. Electron Spectrosc. Relat. Phenom. 21 (1980) 265.

15. K. Hübner, Phys. Stat. Sol. (a) 42 (1977) 501.

TABLE 1

Hydrothermal run parameters

Run	Leachant	Temp. °C	Duration (hours)	A/V[1] (cm^{-1})	Vessel
R1	DDW	300	455	0.15	Au[3]
R2	DDW + SiO_2	175	30	0.1	Parr
R3	"	"	250	"	"
R4	"	"	525	"	"
R6	DDW + SiO_2 (unpurged)	150	290	0.1	"
R7	DDW + SiO_2 (purged)	"	820	"	"
R8	DDW + SiO_2	250	670	2×10^{-3}	SS[2]
R9	"	"	168	"	"
R10	DDW	"	168	0.05	Ag[3]

1 A/V = Ratio of specimen surface area to solution volume.
2 SS = Large stainless steel vessel (1 litre volume).
3 Au = Sealed gold bag in pressurized steel vessel,
Ag = Sealed silver bag in pressurised steel vessel.

TABLE 2

Carbon coverage (at.%)

Run	ΣD = 0	ΣD = 10	ΣD 0 100	ΣD = 1000
Unleached (R0)	15	3	2	2
R1	17	10	6	3
R2	8	7	6	N.D.
R3	6	4	5	3
R4	26	7	3	1
R6	23	16	14	13
R7	34	14	11	11
R8	31	6	6	2
R9	46	20	8	2

TABLE 3

Binding energies and peak splittings for species occurring in $CaTiO_3$ and $CaTiSiO_5$

Species	Xps Peak	Binding Energy (eV)	O 1s Binding Energy	References
Ti metal	$2p_{3/2}$	453.1 (5.5)		
TiO	"	455.1 (5.2)	530.1	[13]
Ti_2O_3	"	456.7 (5.5)	530.1	
TiO_2	"	458.7 (5.8)	530.1	
Ca	$2p_{3/2}$	345.7 (3.7)		
CaO	"	347.1 (3.4)	529.9	[14]
Si	2p	99.0		[8]
SiO_2	"	103.5		
SiO_x $0 < x \leq 2$	"	$99.0 < B.E. \leq 103.5$		[15]

The numbers in parentheses refer to the splitting of doublets as reported in the literature.

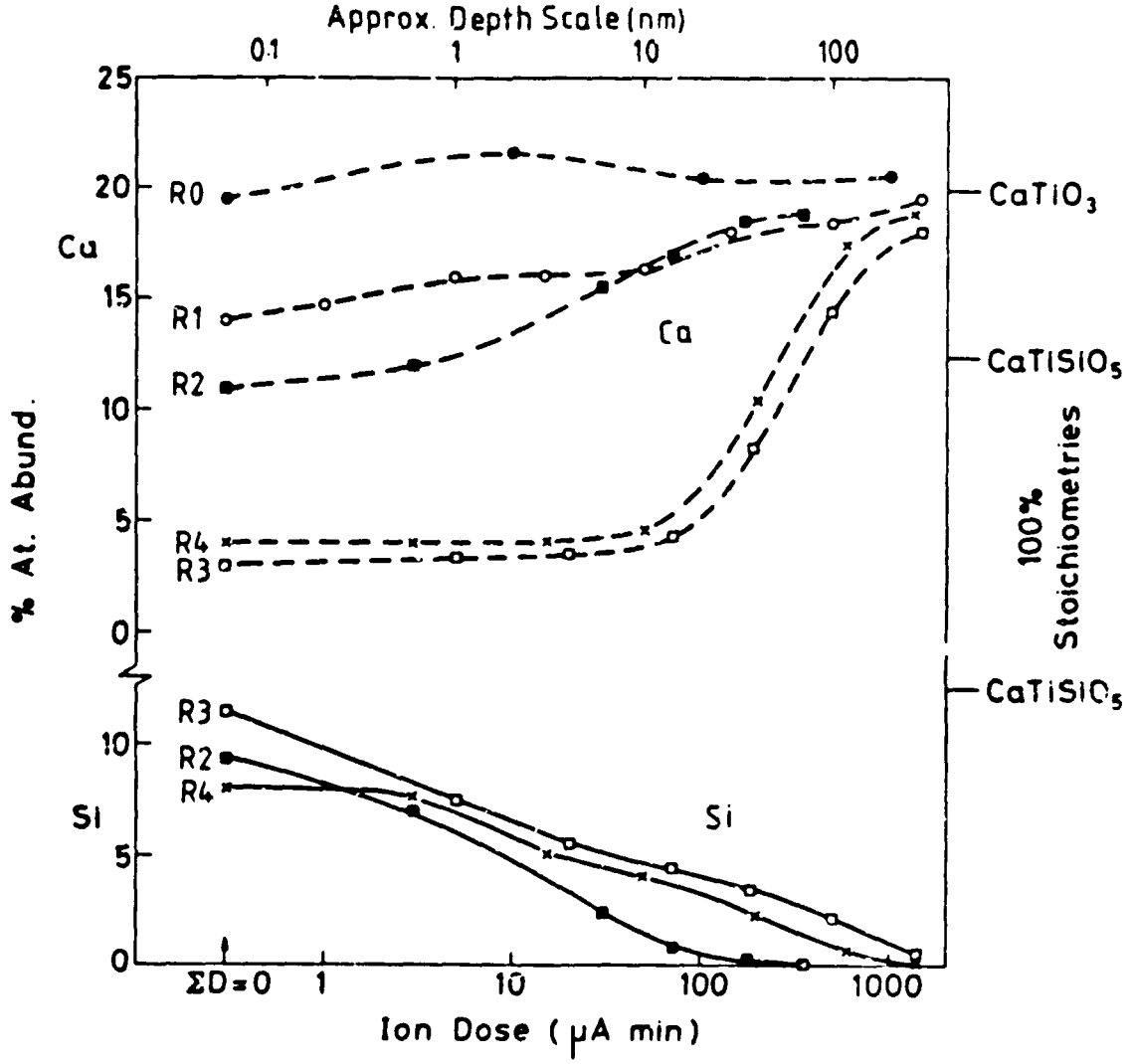

a

AERE R 12390 Fig 1

Abundances of (a) Ca and Si, and (b) Ti and O as functions of ion etching dose. Data are shown for the following surfaces: polished unleached surface (R0) = ●; 455 hrs at 300°C in DDW (R1) = ○; 30 hrs at 175°C in DDW + SiO_2 (R2) = ■; 250 hrs at 175°C in DDW + SiO_2 (R3) = □; and 525 hrs at 175°C in DDW + SiO_2 (R4) = x. The nominal stoichiometries are shown for $CaTiO_3$ and $CaTiSiO_5$. An approximate depth scale is shown on the top horizontal axis.

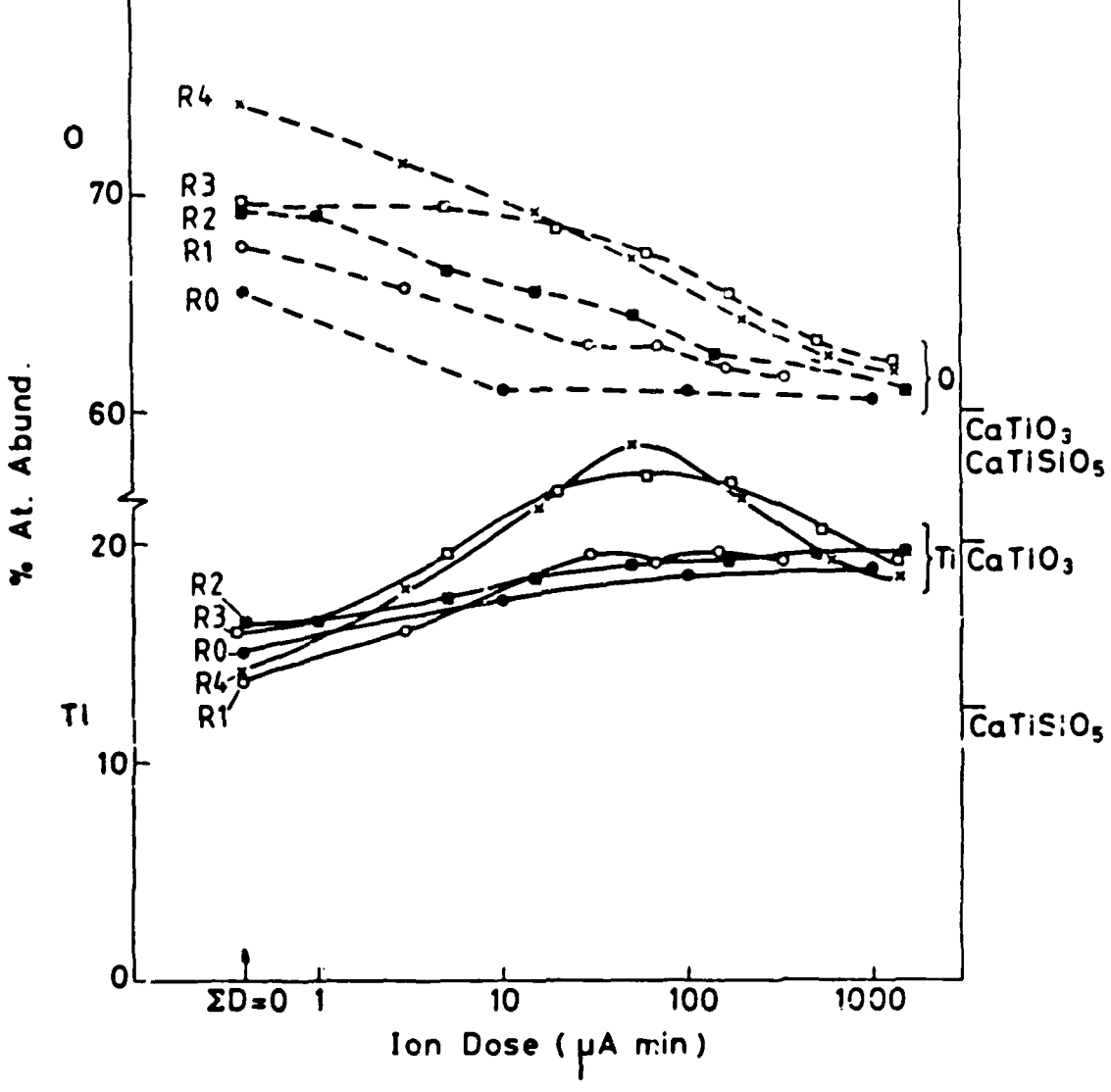
Approx. Depth Scale (nm)
01
1
10
100
80
70
60
20
10
0
O
Ti
% At. Abund.
R4
R3
R2
R1
R0
R2
R3
R0
R4
R1
O
Ti
CaTiO3
CaTiSiO5
CaTiO3
CaTiSiO5
ΣD=0
1
10
100
1000
Ion Dose (μA min)

b

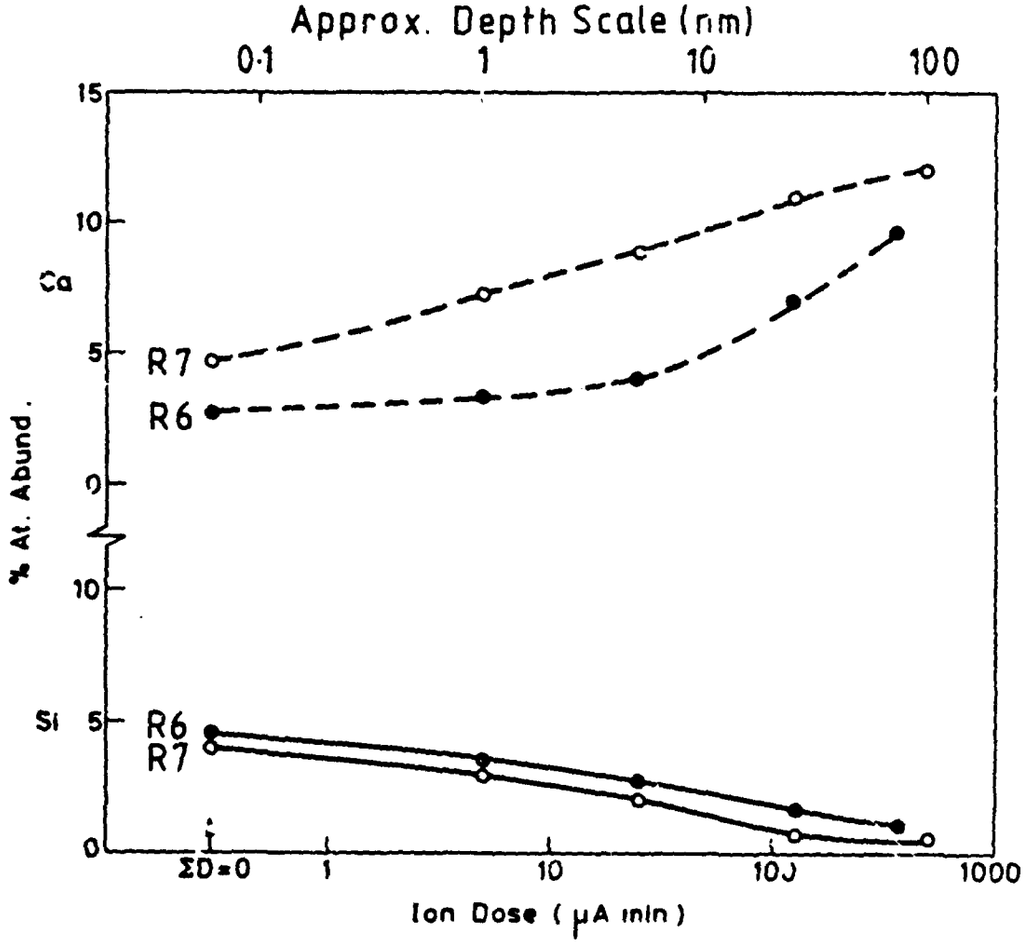

a

AERE R 12390 Fig. 2

Abundances of (a) Ca and Si, and (b) Ti and O as functions of ion etching dose. The effect of purging absorbed CO_2 from the leachant is investigated. 290 hrs at 150°C in DDW + SiO_2 (unpurged) (R6) = ● and 820 hrs at 150°C in DDW + SiO_2 (purged) (R7) = ○.

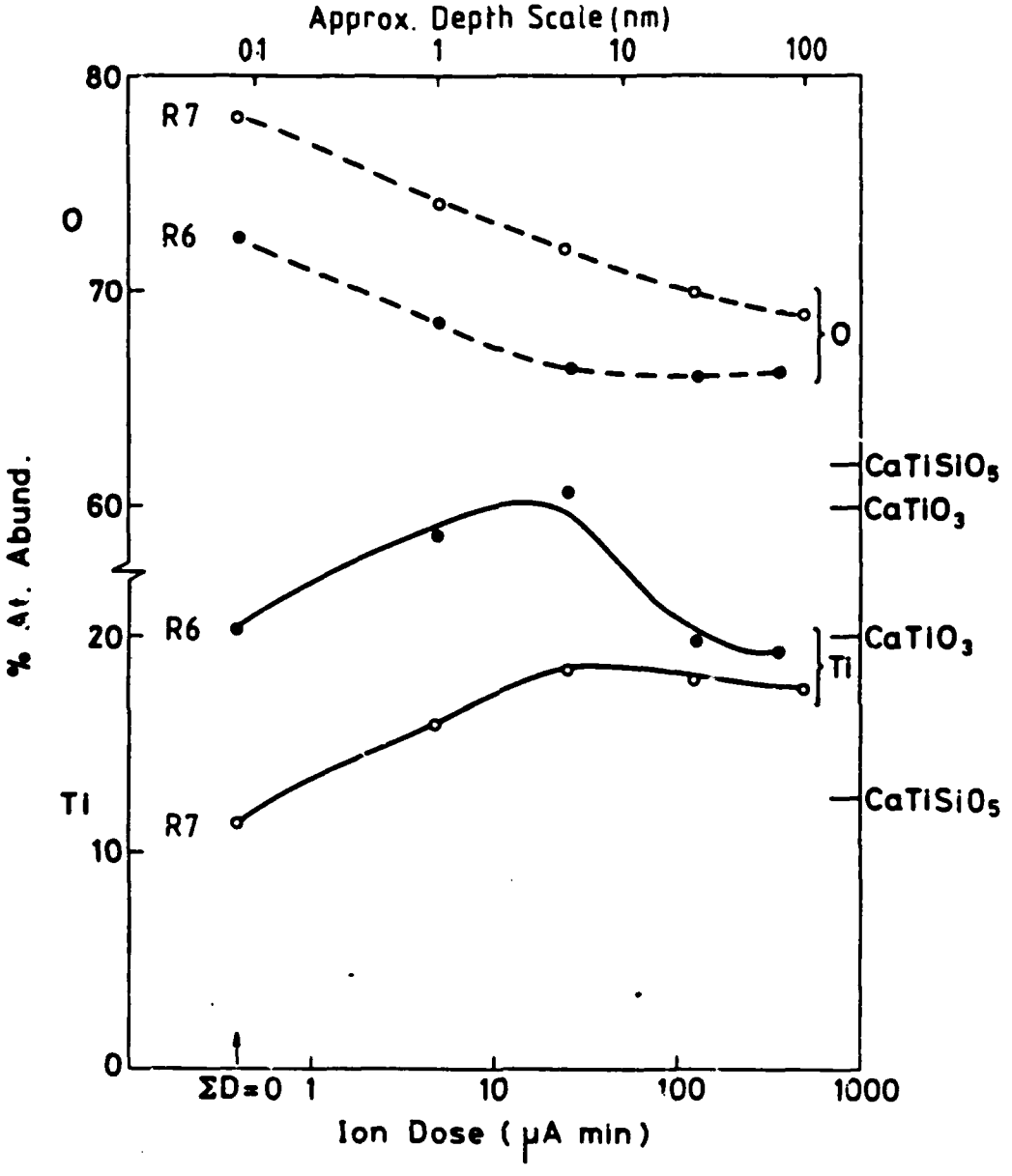
Approx. Depth Scale (nm)
0.1
1
10
100
80
R7
O
R6
70
O
CaTiSiO5
60
CaTiO3
% At. Abund.
20
R6
CaTiO3
Ti
Ti
R7
CaTiSiO5
10
0
ΣD=0
1
10
100
1000
Ion Dose (μA min)

b

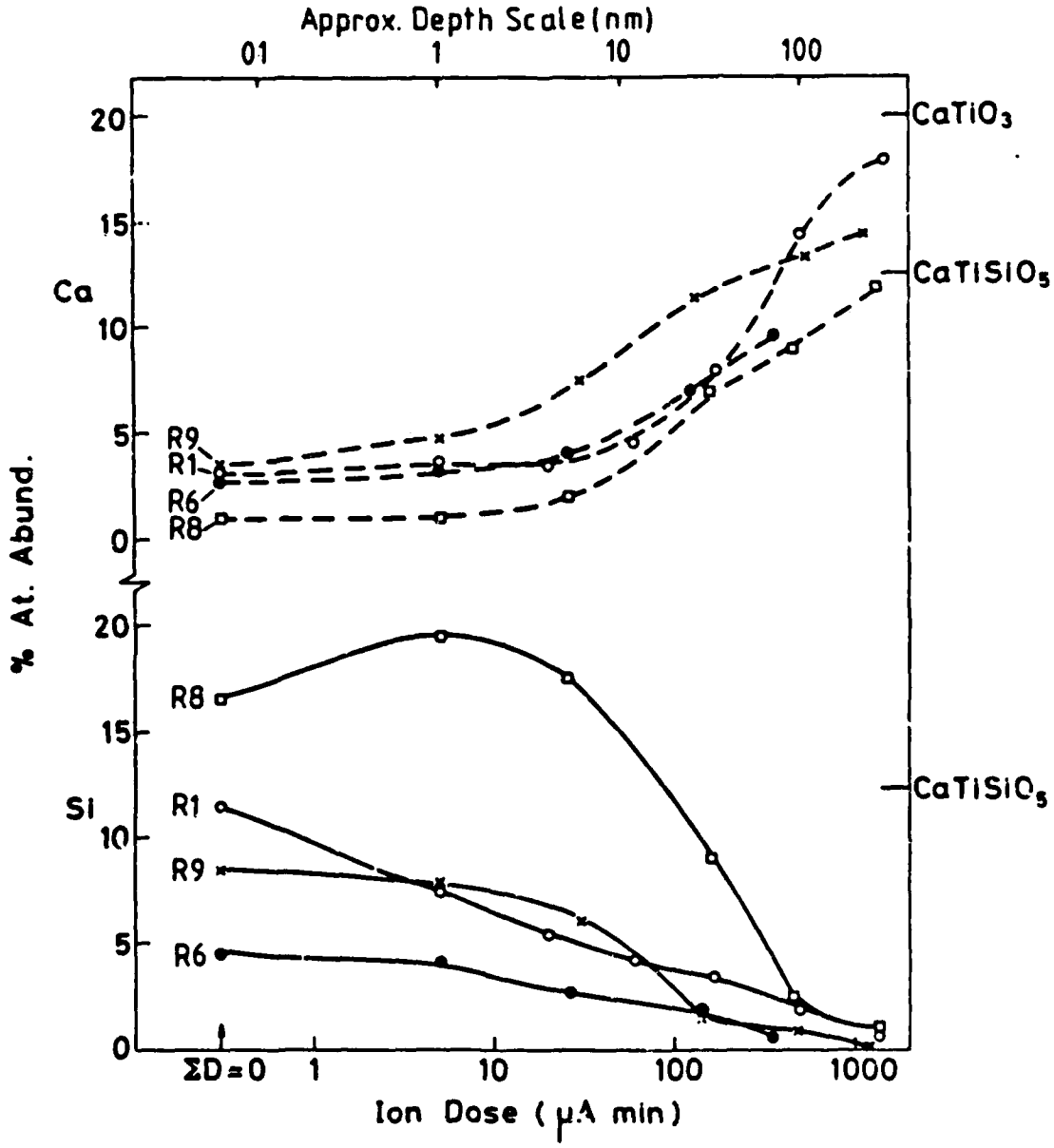

a

AERE R 12390 Fig. 3

Abundances of (a) Ca and Si, and (b) Ti and O as functions of ion etching dose. The effect of temperature is investigated. 290 hrs at 150°C in DDW + SiO_2 (R6) = •; 250 hrs at 175°C in DDW + SiO_2 (P3) = o; 168 hrs at 250°C in DDW + SiO_2 (R9) = x; 670 hrs in DDW + SiO_2 (R8) = □.

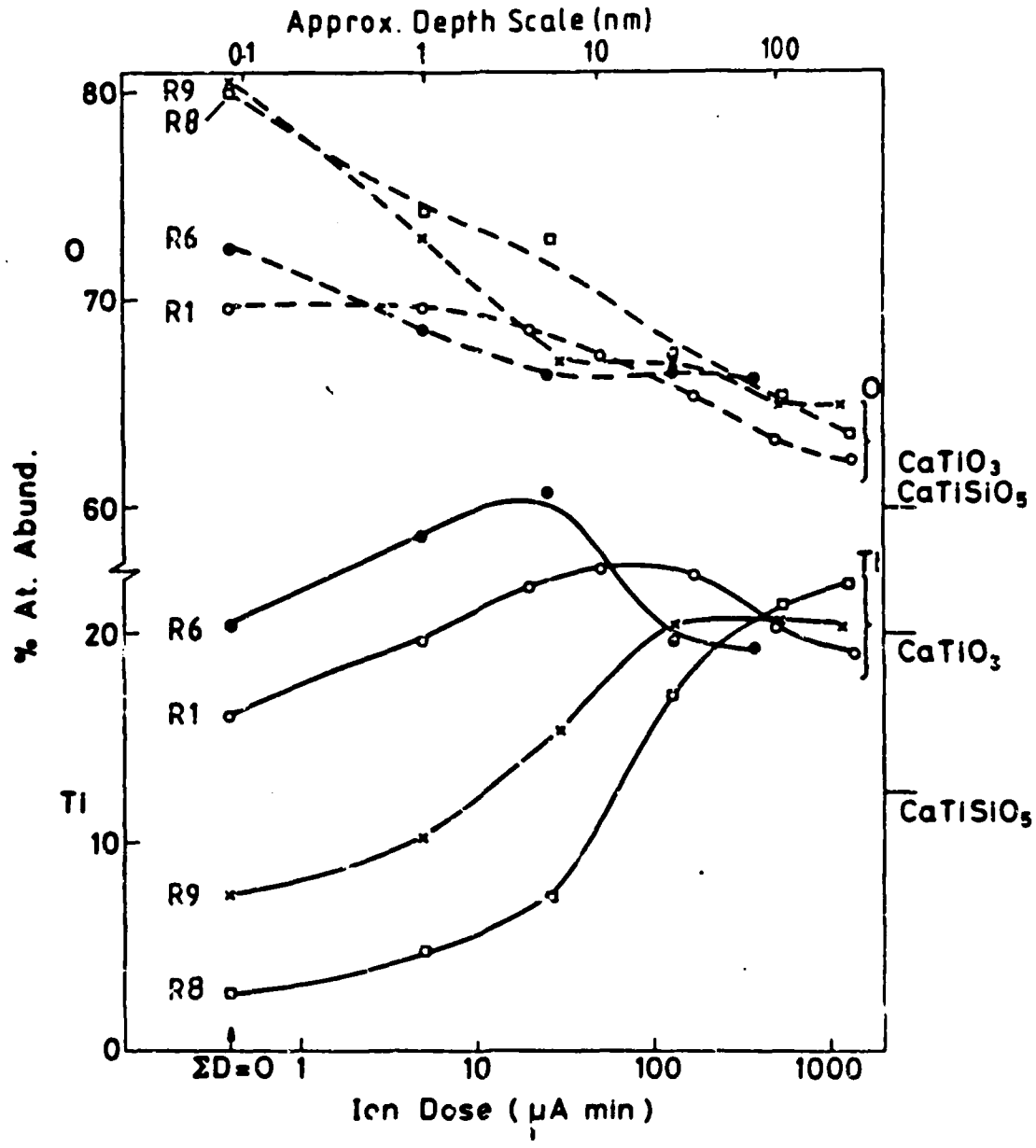
Approx. Depth Scale (nm)
0.1
1
10
100
80
70
60
20
10
0
O
Ti
% At. Abund.
R9
R8
R6
R1
R6
R1
R9
R8
O
Ti
CaTiO3
CaTiSiO5
CaTiO3
CaTiSiO5
ΣD=0
1
10
100
1000
Ion Dose (μA min)

b

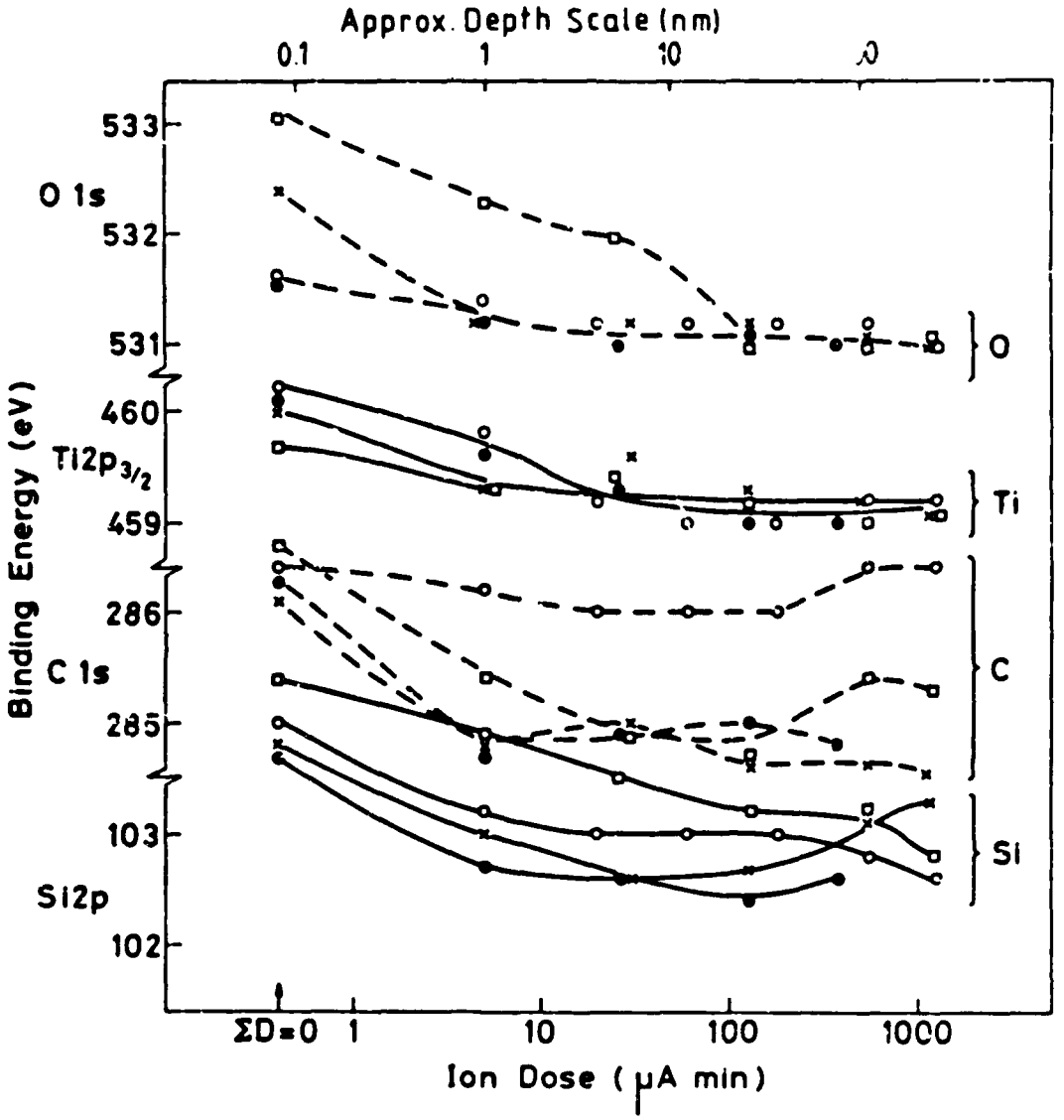

AERE R 12390 Fig. 4

Binding energies of O 1s, Ti $2p_{3/2}$, C 1s and Si 2p electrons as functions of ion etching dose for an unleached specimen (R0) = •; (R1) = ○; (R2) = ■; (R3) = □; and (R4) = x. Run conditions are listed in Table 1 and in caption for Figure 1.

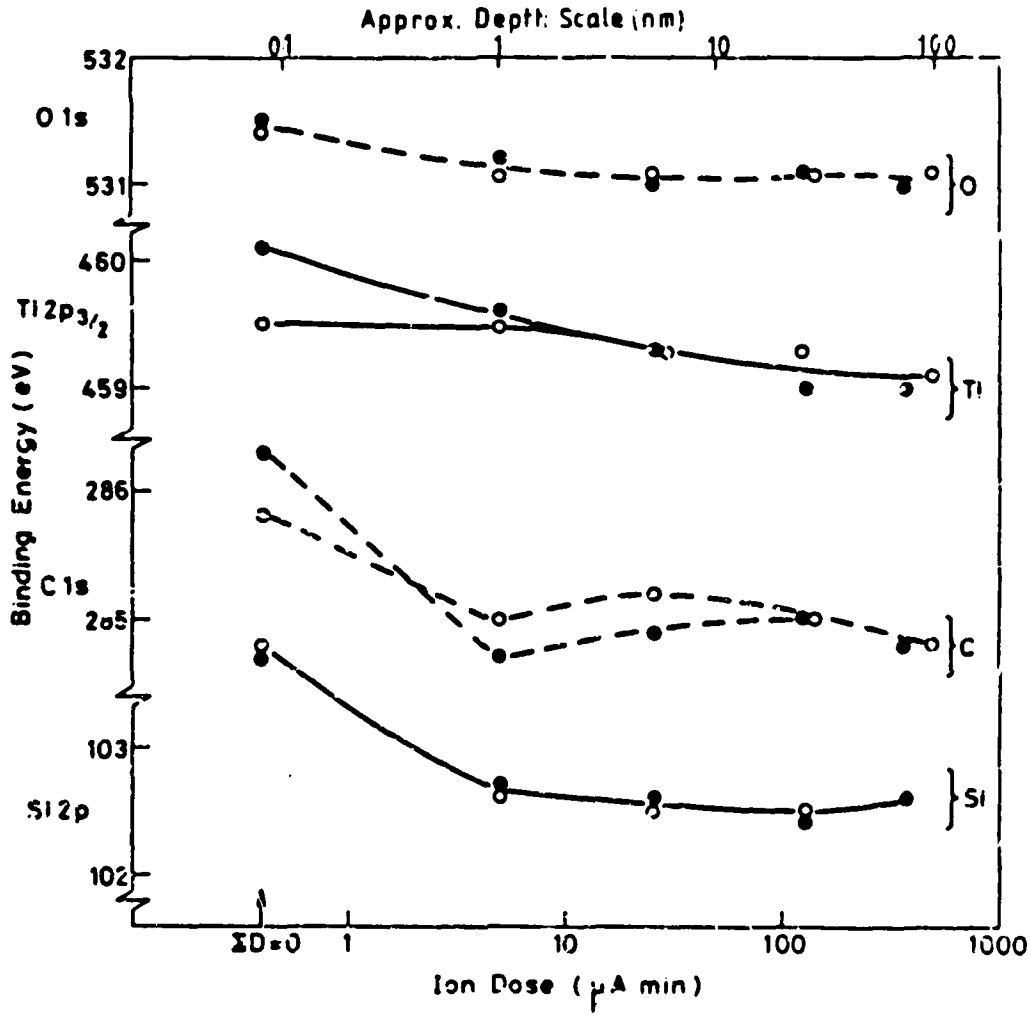

a

AERE R 12390 Fig. 5

Binding energies as functions of ion etching dose (R6) = • and (R7) = ○, are shown in (a) and (R3) = ○; (R6) = •; (R8) = □; and (R9) = x are shown in (b). Run conditions are listed in Table 1 and Figures 2 and 3.

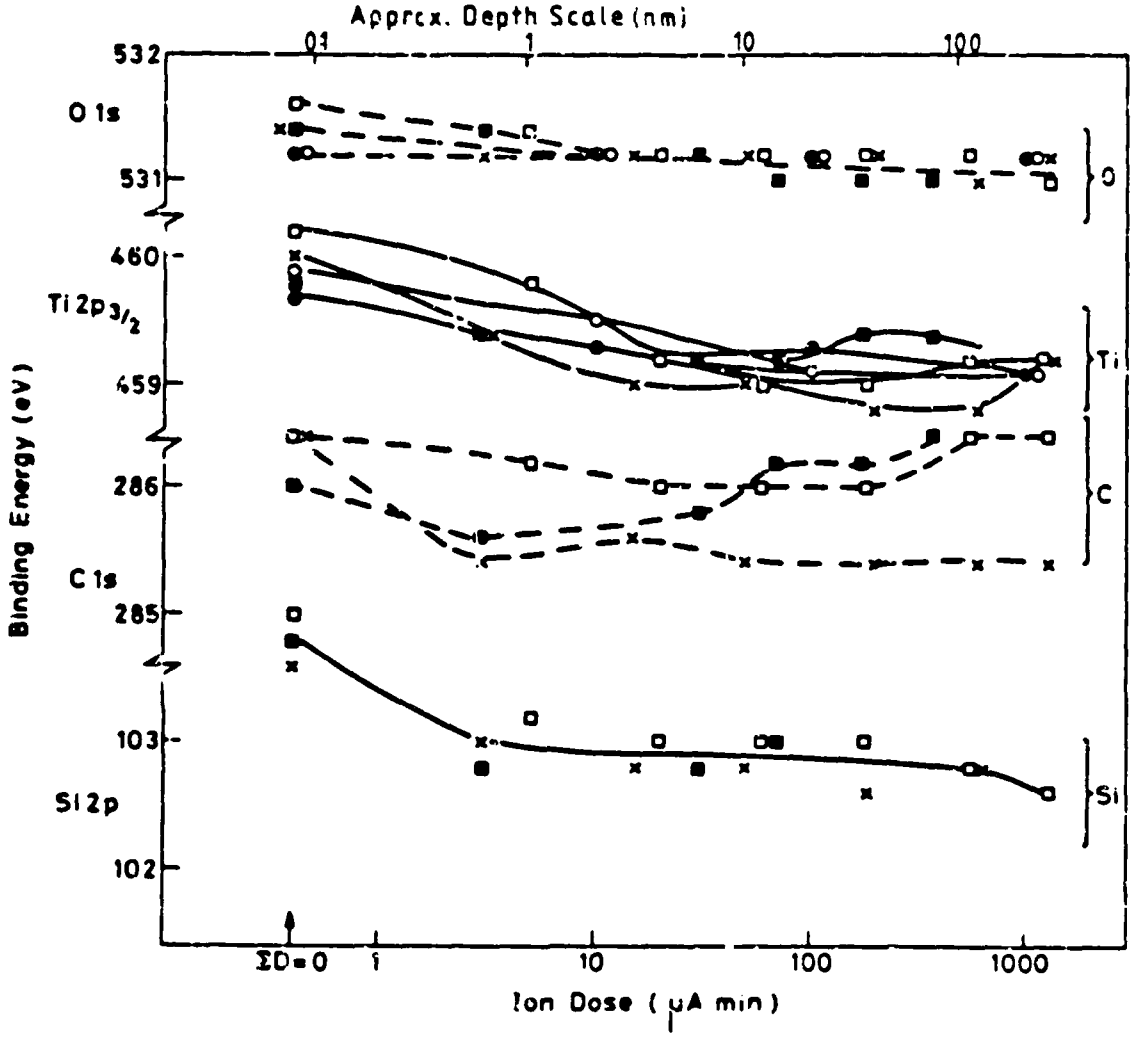
Approx. Depth Scale (nm)
0.1
1
10
100
532
O 1s
531
460
Ti 2p3/2
459
286
C 1s
285
103
Si 2p
102
Binding Energy (eV)
O
Ti
C
Si
ΣD=0
1
10
100
1000
Ion Dose (μA min)

b

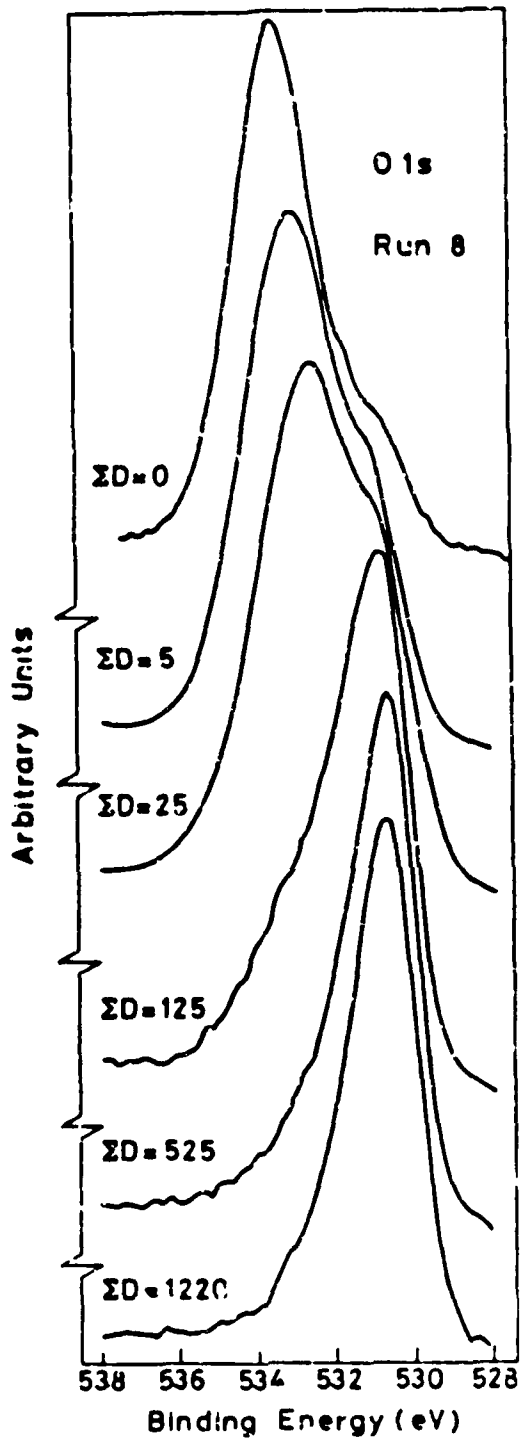

AERE R 12390 Fig 6

Evolution of O 1s envelope as function of ion etching dose for R8, showing charge shifted peak due to either the presence of precipitated titanate on attacked surface, or a precipitated siliceous layer.

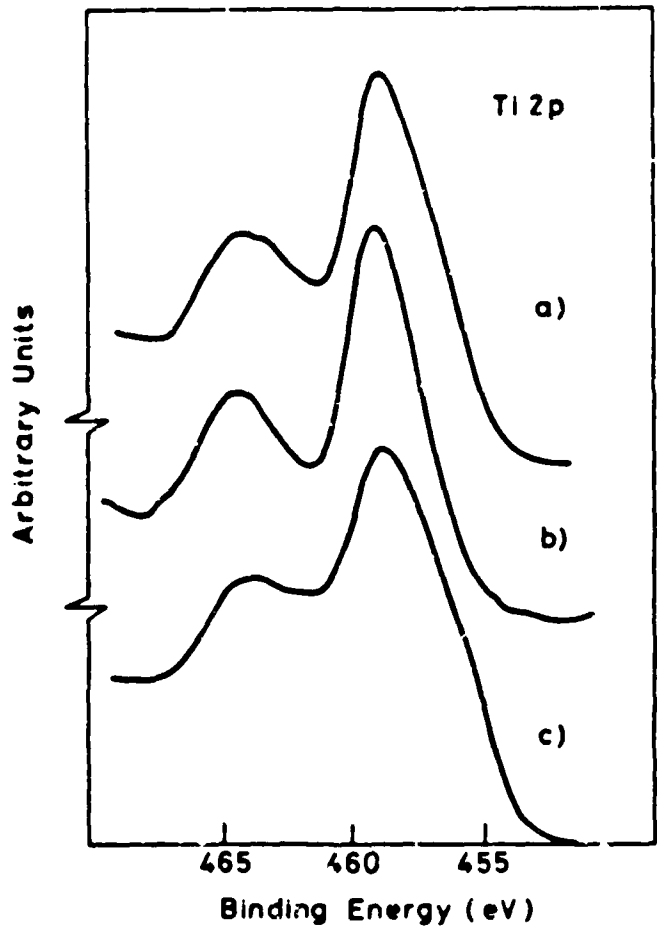

AERE R 12390 Fig. 7

Experimental Ti 2p envelopes for (a) polished unleached surface (R0), (b) 300°C for 455 hrs in DDW (R1) and (c) 175°C for 250 hrs in DDW + SiO_2 after $\Sigma D = 100$ μA min.

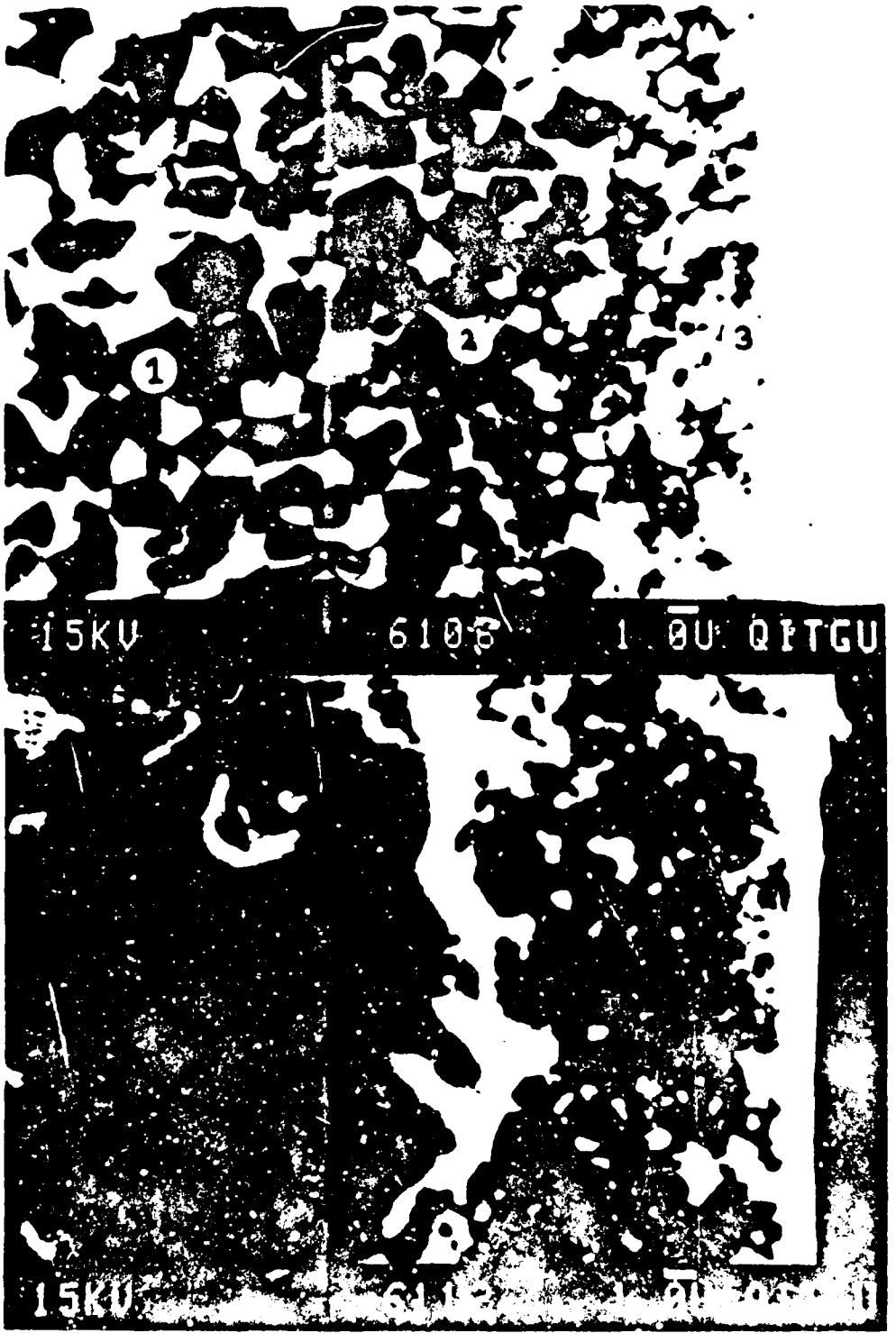

AERE R 12390 Fig. 8

SEM micrographs of fracture face of perovskite (R10) after 7 days in DDW at 250°C. (a) and (b) [illegible]

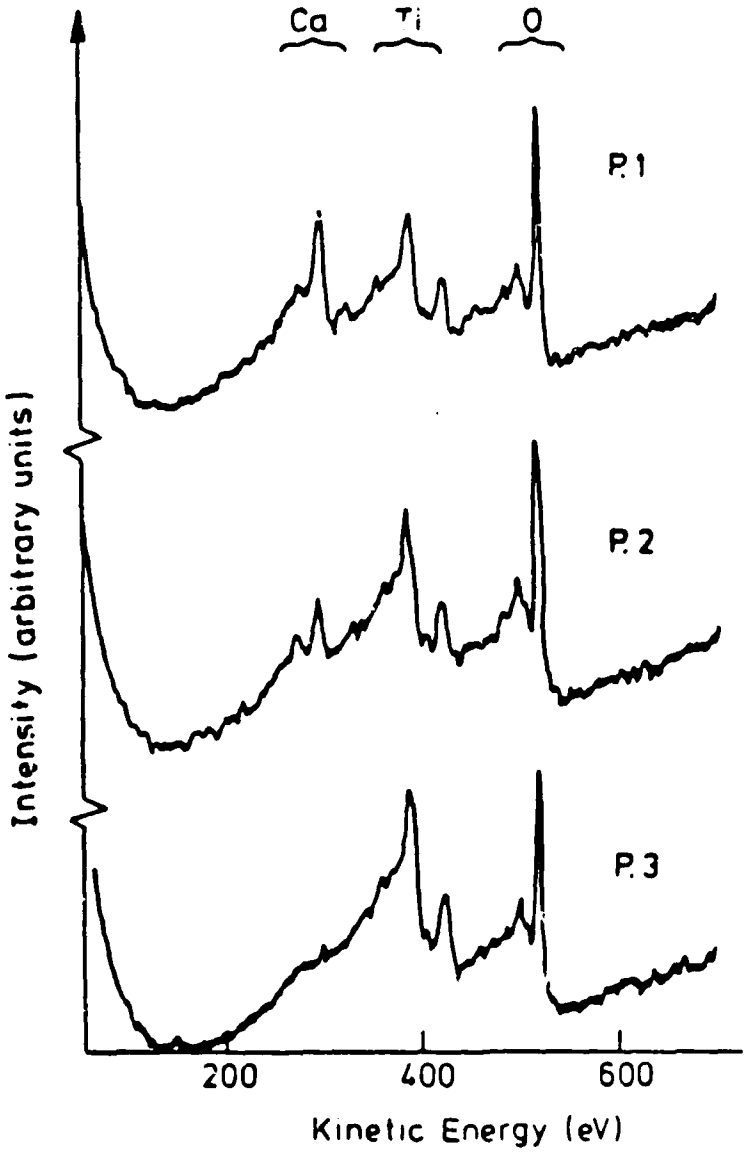

AERE R 12390 Fig. 9

AES point scans on perovskite fracture face. Top scan is for P1 (Figure 8(a)) in the perovskite substrate, middle scan is for P2 at the substrate/precipitate interface and the bottom scan is for P3 in the precipitate layer.

END

DATE

FILMED

5-88

DTIC